

Accounting for physical barriers in species distribution modeling with non-stationary spatial random effects

Haakon Bakka¹, Jarno Vanhatalo², Janine Illian³, Daniel Simpson⁴, and Håvard Rue¹

¹*Department of Mathematical Sciences, Norwegian University of Science and Technology*

²*Department of Mathematics and Statistics, and Department of Biosciences, University of Helsinki*

³*Centre for Research into Ecological and Environmental Modelling, School of Mathematics and Statistics, University of St Andrews, Scotland, UK*

⁴*Department of Mathematical Sciences, University of Bath, BA2 7AY, United Kingdom*

October 25, 2021

Abstract

This paper is motivated by a study on the spatial distribution of fish larvae in reproduction habitats of three commercially important fish species in the Finnish archipelago. Species distribution modeling (SDM) requires realistic models that account for spatial dependence in observation data that cannot be explained by environmental factors alone.

Gaussian latent variable models are increasingly used in this context, where a stationary Gaussian random field accounts, for instance, for the spatial correlation driven by unmeasured covariates. In this paper we challenge the assumption of stationarity in cases where there are physical barriers in the study area, such as when our interest is in fish populations near the coast. In these situations, the common assumption of stationary second order spatial behaviour is likely to be unrealistic, as spatial dependencies should be considered around the barriers rather than across them.

We develop a non-stationary Gaussian field that treats, e.g., land as a barrier to spatial correlation. We define the field as a continuous solution to a differential equation with spatially varying coefficients, and achieve a computational cost similar to that of the stationary model. We demonstrate the benefits of the new model for a fish larvae application in the Finnish archipelago.

1 Introductions

Species distribution models are a key part in ecologists' toolbox. They are increasingly used to improve our understanding of species habitat preferences (Latimer et al., 2006; Austin, 2007) and species interactions (Ovaskainen et al., 2015), to identify and manage conservation areas (Johnston et al., 2015) and to predict the response of species to climate change (Clark et al., 2014). The main modeling objective in these contexts is to use information on the occurrence (or abundance) of a species and the associated environment to infer information on the relationship between these two attributes (Gelfand et al., 2006; Latimer et al., 2006). When information on environmental characteristics is available from unsampled locations, it may then be used to predict the abundance of a species over a region of study to build thematic species distribution maps (Elith and Leathwick, 2009; Gelfand et al., 2006).

Species distribution modeling is directly related to a specification of a species' response to a suite of environmental factors (Latimer et al., 2006), which is traditionally done using generalized linear or additive models (Gelfand et al., 2006; Guisan et al., 2002). However, current environmental conditions alone may not sufficiently explain species distribution (Latimer et al., 2006). There may be spatial dependence in the measurement process and some environmental factors are not measured *in situ*

but they are available as thematic raster maps which introduces misalignment between the sampling locations and the environmental data (Gelfand et al., 2006). Often these rasters are also a product of intermediate modeling and may not adequately represent the true environment at a sampling location (Vanhatalo et al., 2012). Moreover, ecological processes such as dispersal, competition and the dynamics of populations also affect the spatial distribution of species. For example, as a result of competition with other individuals species may diffuse from location with optimal habitat to less optimal habitat close by. For these reasons, hierarchical generalized models that include spatial random effects to account for unexplained spatial dependence in the data have gained increasing interest among species distribution modelers (Latimer et al., 2006; Vanhatalo et al., 2012; Ovaskainen et al., 2015).

Spatial random effects, such as Gaussian random fields, can be used to account for the spatially structured autocorrelation that arises from associations unexplained by the available covariates (Elith and Leathwick, 2009; Latimer et al., 2006). In other words, the spatial random effect compensates for model misspecification when measurements are not conditionally independent given the fixed effects. Assuming that all the noise is independent, i.e. using a model without a spatial effect, will often result in too narrow credible intervals, because measurements are taken to be less dependent than they are. It can also systematically bias estimates of spatial fixed effects. By mapping the posterior distribution of the spatial random effect one can derive hypotheses concerning factors explaining these patterns. The spatial random effect may also improve the predictions both within the spatial area covered by sampling (interpolation) and further away from the sampling areas (extrapolation) (Vanhatalo et al., 2012; Kalliasvuori et al., 2016). The former is evident since the spatial random effect alone is powerful in interpolation as shown by the vast literature on Kriging and Bayesian spatial modeling (see, e.g., Gelfand et al., 2010, for general treatment and references). A spatial random effect may improve the model’s extrapolation performance, if its involvement in the model improves the posterior estimates for the fixed effects according to which the extrapolation has to be conducted (Kennedy and O’Hagan, 2001).

The core characteristic of a Gaussian random field is its covariance function, which describes the spatial autocorrelation as a function of spatial location. The spatial autocorrelation is assumed to be stronger in close proximity to a location than further away. In addition, stationarity is commonly assumed, i.e. that the correlation depends only on the distance between the points, but neither on the direction nor on the spatial coordinates. Typically, the stationarity assumption is made for practical reasons since constructing and inferring interpretable non-stationary covariance functions is challenging (Paciorek and Schervish, 2006). However, this assumption may severely violate the properties of the modeled region and lead to bias in model results. For example, physical barriers such as roads, mountains and lakes in terrestrial domain and islands and peninsulas in aquatic environments, pose obstacles for species movement and dispersal. Hence, the spatial correlation should not take the shortest path going across such obstacles, which is exactly what happens with a stationary model, but should travel around them.

Different solutions for this barrier problem have been discussed by Ramsay (2002) from a spline smoothing view, and by Wood et al. (2008) with a similar focus as the current paper. For the models presented therein, the holes and boundaries are barriers in our terminology. The paper by Scott-Hayward et al. (2014) develops another solution to this problem, and its introduction gives a good overview of the difficulties involved in trying to compute distances around barriers. Our approach, however, avoids all of these difficulties as we construct the model in a different framework. This allows us to provide a solution that has an advantage to the above methods in its intuitive nature and its ease of use. Another possible approach is to compute the covariance matrix through shortest distance, by using the algorithm of Dijkstra (1959) on a fine grid. This idea of shortest path has been mentioned in verbal discussions, but we have found no appropriate references for its statistical use. In the Gaussian process (Gaussian random field) literature non-stationarity is typically obtained by constructing non-stationary covariance functions by, e.g., kernel convolution (Higdon, 1998) or locally varying geometric anisotropies (Paciorek and Schervish, 2006). We believe these methods

could also be used to construct solutions to the barrier problem.

In this paper, we challenge the assumption of stationarity in the spatial random field, and introduce a non-stationary Gaussian field that forces spatial correlation to go around barriers in the study area. In particular, we consider a situation where the study area consists of two regions where we assign separate range parameters to each of the regions, i.e. the distance at which spatial correlation is no longer significant varies among those regions. The core idea, that then allows us to account for barriers, is to define a barrier region where the range parameter is almost zero. This is achieved by defining the field as a continuous solution to a differential equation with spatially varying coefficients. The local averaging structure is defined through manipulating these coefficients. This idea is a generalization of the SPDE approach by Lindgren et al. (2011). Using the same tools as Lindgren et al. (2011), we achieve a computational cost similar to the stationary model, hence making model fitting practically feasible. We include the new model in a completely specified Bayesian framework, and interpret all the parameters.

This approach is different from one based on Dijkstra’s algorithm both in the definition of the correlation distance and in computational cost. Specifically, the correlation distance considered in our modeling approach is not equivalent to the shortest distance but is closer to an average over the short paths (see Figure 4). In addition, in applications with a large number of data locations (10 000 or more) computing the distances from all nodes to all other nodes is very expensive, even with Dijkstra’s algorithm, and even just storing the full spatial covariance matrix is quite expensive. Our approach represents the spatial field with a sparse precision matrix (inverse covariance). This facilitates model fitting for large datasets.

We demonstrate the benefits from using our non-stationary Gaussian field compared to the stationary alternative with a case study on the distribution of fish larvae in the Finnish archipelago. We analyze the distribution of three species of fish larvae and show that the non-stationary Gaussian field changes the model’s inference on the fixed effects. There are also significant changes in the posterior spatial fields. Here, the new model separates points that the stationary model would consider close despite a physical land barrier between them. This has two visible effects; a lack of smoothing across land, and, increased posterior uncertainty in inlets without nearby measurements.

2 The case study area and data

The study area is located in the Archipelago Sea on the south-west coast of Finland in the northern Baltic Sea (Figure 1). The Baltic Sea is one of the largest brackish water bodies in the world consisting of shallow, topographically complex and extensive archipelago rich in islands. Environmental gradients are typically strong, both north-southward and west-eastward along the coastline but also from inshore to offshore, e.g. spring-time temperature sum and turbidity vary strongly between inner bays and open water area due to the influence of river runoff. The archipelago and coastal areas host many essential biological processes such as fish reproduction. Hence, knowledge on the specific reproduction areas is of central importance in marine spatial planning and fisheries management (Vanhatalo et al., 2012).

As a case study we consider three species of fish, smelt (*Osmerus eperlanus*), perch (*Perca fluviatilis*) and pikeperch (*Sander lucioperca*). They are of freshwater origin and spawn in shallow coastal waters in low salinity estuaries and river mouths in the northern Baltic Sea (Shpilev et al., 2005; Bergström et al., 2014). They are fished commercially and are also highly sought after by recreational fishers. Our main interest is in the early-stage larvae, which are found relatively close to the spawning sites. We use a subset of data (198 sampling locations) introduced by Kallasvuori et al. (2016). The data were collected in 2007 and 2011 and comprise of the number of larvae per sampling location together with information on varying sampling effort (measured as the volume of water sampled). The environmental variables included six variables, which were available in GIS format in 50m resolution throughout the study area, and spatial coordinates (see Table 1). Sampling

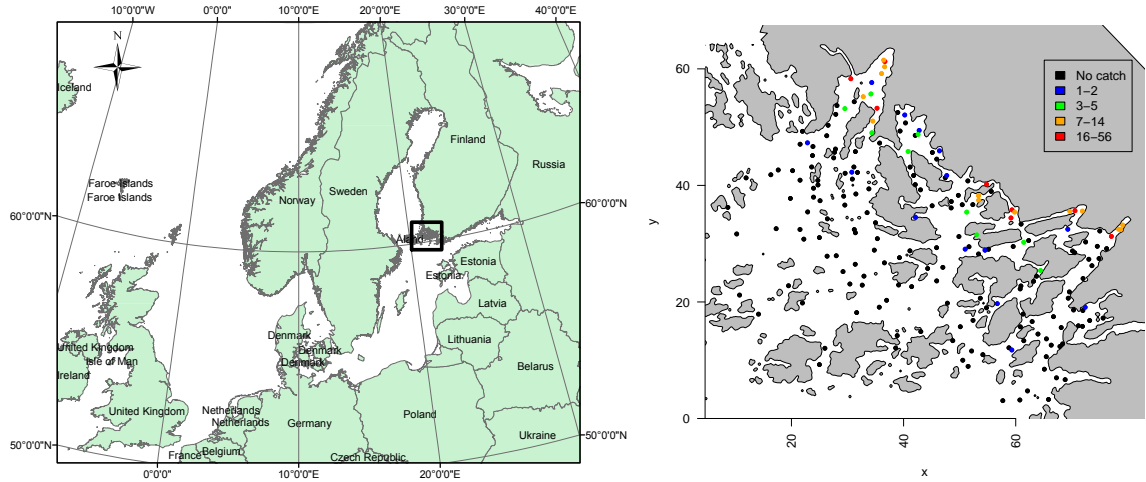


Figure 1: The study area with smelt larvae observations.

year was also available, but not included, as there were only two unique values, and the exploratory data analysis did not indicate any differences between years. If the study had contained more years, it would have been natural to include a temporal model component in the model, as in Kallasvuo et al. (2016).

The covariates, except for RiverFlow, were standardized to have mean zero and variance 1 before the analysis. This was mainly done in order to facilitate interpretation of the estimates and the uncertainty of the fixed effects. This also implies that due to standardization the priors act in the same way on all fixed effects. The response of smelt abundance along the covariate RiverFlow was step-like in the analysis of Kallasvuo et al. (2016), which comprised the whole coastline of Finland. In our sub-area, 193 sites out of all 198 sites took on a total of only two different values. It is unlikely that a meaningful linear relationship can be derived given these values, and hence, we recoded the covariate as a factor covariate in this study, where 0 represents the values 0.08 or less and 1 represents values greater than 0.08.

Figure 1 shows the data values in space, and the structure of the archipelago. For the remainder of this paper one unit on the spatial scale will refer to one kilometer. For the main case study, we discuss only the smelt data in detail, both with and without covariates, to illustrate how the new model behaves compared to the stationary model. After that we fit the model to all three species, both with and without covariates.

3 Methods

3.1 The structure of the model

We model the number of larvae, y_i , at sampling location s_i ($i = 1, \dots, n$) with a latent Gaussian model (that is, a generalized linear model with random effects). The first level is the observation model, where the Poisson distribution has been chosen because we have count data with continuous sampling effort. For other SDM applications it would be natural to use a different observation model (including a different link function); e.g. a Gaussian observation model for biomass data or a Bernoulli

Name	Covariate description
AverageDepth	Average depth in a circle of 15 km; describes the water depth gradient in a large spatial scale.
Dist30m	Distance to 30 m depth zone; implicates location in the archipelago so that, e.g. sheltered inner bays are emphasized by this covariate.
RiverFlow	Square root of inverse distance to nearest river mouth weighted with annual average runoff; describes the influence of the river mouths and freshwater runoff.
lined15km	Shoreline length in a circle of 15 km; describes the effect of wind exposure and water exchange.
Openness	\log_{10} of wave exposure; describes the degree of wave exposure
TempSum	Cumulative temperature sum from ice-break to July 15; describes how rapidly water area warms up in spring after ice break-up.

Table 1: Covariates used in the models.

model for presence-absence data. The hierarchical model is

$$y_i | \eta_i \sim \text{Poisson}(z_i e^{\eta_i}) \quad (1)$$

$$\eta_i = \beta_0 + \vec{x}_i \vec{\beta} + u(s_i) + \epsilon_i \quad (2)$$

$$\beta_j \sim \mathcal{N}(0, 1000) \quad (3)$$

$$\beta_0 \sim \mathcal{N}(0, 1000) \quad (4)$$

$$\epsilon_i \sim \mathcal{N}(0, \sigma_\epsilon^2) \quad (5)$$

where the observations are assumed to be conditionally independent given the latent variable $\vec{\eta}$ (which corresponds to the log intensities) and the fixed sampling effort z_i . The vector \vec{x}_i contains the covariate values, $\vec{\beta}$ is the vector of fixed effects, β_0 is the intercept $u(s)$ denotes the spatial random effect, and ϵ_i is the iid random effect. We consider two spatial random effects: a stationary Matérn random field, see Section 3.2, and a non-stationary field with barriers, see Section 3.3.

The second level describes the latent variable $\vec{\eta}$, also called the linear predictor. Typically in ecological data the assumption of linear relationship between mean and variance in the observation process, implied by the Poisson distribution, is too restrictive (Lindén and Mäntyniemi., 2011). This extra variation (overdispersion) over the Poisson distribution, arising from, e.g., aggregation behavior of individuals, and sampling variability, is modeled with the iid random effect ϵ_i . The spatial random effect, $u(s)$, models spatial variability, such as diffusion and spatial aggregation of the species, effect of covariates that have not been accounted for, and spatially correlated measurement errors.

The third level describes the priors for hyper-parameters $\sigma_\epsilon, \sigma_u$ and r , where the last two are parameters uniquely defining the covariance structure of $u(s)$ as detailed in Sections 3.2 and 3.3. The hyper-parameters change the structure of the model in fundamental ways. The two standard deviation parameters define the signal-to-noise ratio, and the spatial noise to independent noise ratio. The parameter r changes the length scale at which we are studying the spatial dependencies. Both random effects have an effective number of parameters that increases with the number of observations, thus there is a risk of overfitting. Since the effective number of parameters is determined by the values of the hyper-parameters, we can control the overfitting through weakly informative priors on these. We will come back to these priors, and a more detailed interpretation of the hyper-parameters, in section 3.4.

3.2 Stationary spatial random effect

The Matérn field has a long history of successful use, and is considered to have good properties for spatial applications (e.g., Gelfand et al., 2010). The Matérn field is a Gaussian random field, i.e. a continuously indexed random variable where the indices are a subset of \mathbb{R}^n , and any finite collection of indices gives variables that are jointly multivariate Gaussian. The Matérn field can be represented in several ways, of which we will consider two. The first is by giving the covariance as a function of distance between two points. To easily interpret this, we parametrise the Matérn field with the range r , in such a way that the correlation between two points that are r units apart is near 0.1. Letting d be the distance between two arbitrary points, $d = \|s_i - s_j\|$, the covariance function can be written

$$C(d) = \sigma_u^2 \frac{d\sqrt{8}}{r} K_1 \left(\frac{d\sqrt{8}}{r} \right), \quad (6)$$

Here, σ_u and r are constants, and K_1 is the modified Bessel function of the second kind. The subscript on σ_u clarifies that this is the marginal standard deviation of the model component u . Note that we have re-parametrised the traditional Matérn covariance function with range $r = \rho/\sqrt{8}$ where ρ is the traditional length scale parameter (e.g., Gelfand et al., 2010). We continue to use this parameter r in the following equations.

The second representation of the Matérn field is as a (weak) stationary solution $u(s)$ to the stochastic partial differential equation

$$u(s) - \nabla \cdot \frac{r^2}{8} \nabla u(s) = r \sqrt{\frac{\pi}{2}} \sigma_u \mathcal{W}(s), \quad (7)$$

where $u(s)$, $s \in \Omega \subseteq \mathbb{R}^2$ is the Gaussian field, r and σ_u the same constants as earlier, $\nabla = \left(\frac{\partial}{\partial x}, \frac{\partial}{\partial y} \right)$, and $\mathcal{W}(s)$ denotes white noise. The details of this last representation, including how to solve it, i.e. how to compute the precision matrix for $\vec{u} = (u(s_i))_i$, can be found in Lindgren et al. (2011). Note that we have re-parametrised their equation (2) and fixed $\alpha = 2$. For the special case we are interested in, we include the details on how to solve the equation in Appendix A.

3.3 Spatial random effect with barrier

The new barrier model is represented by a non-stationary Gaussian field. The idea is to define the field locally, with one governing equation for the normal area, and another for the barrier area. The range r_b in the barrier area is given a fixed value close to zero, while the range in the normal area is a hyper-parameter in the inference. In the case study presented in section 2, water/ocean is considered the normal area, while land is considered the barrier area. In other applications, normal may be, e.g. plains or forests, and barrier may be, e.g., human settlements or rivers.

Define $u(s)$ to be the (approximation of the) continuous weak solution to

$$\begin{aligned} u(s) - \nabla \cdot \frac{r^2}{8} \nabla u(s) &= r \sqrt{\frac{\pi}{2}} \sigma_u \mathcal{W}(s), \text{ for } s \in \Omega_n \\ u(s) - \nabla \cdot \frac{r_b^2}{8} \nabla u(s) &= r_b \sqrt{\frac{\pi}{2}} \sigma_u \mathcal{W}(s), \text{ for } s \in \Omega_b, \end{aligned}$$

where Ω_n is the normal terrain, Ω_b is the barrier, and their disjoint union gives the whole study area. Mathematical details for the solution can be found in appendix A.

Why does this yield the behavior we desire? These equations represent a local averaging of nearby values. If you have two points, with a lot of land in between, the range-almost-zero property stops the local averaging on the barrier. Intuitively, this forces the correlation to go around the barrier area, following the normal area where you are still taking local averages. Figure 2 illustrates that the

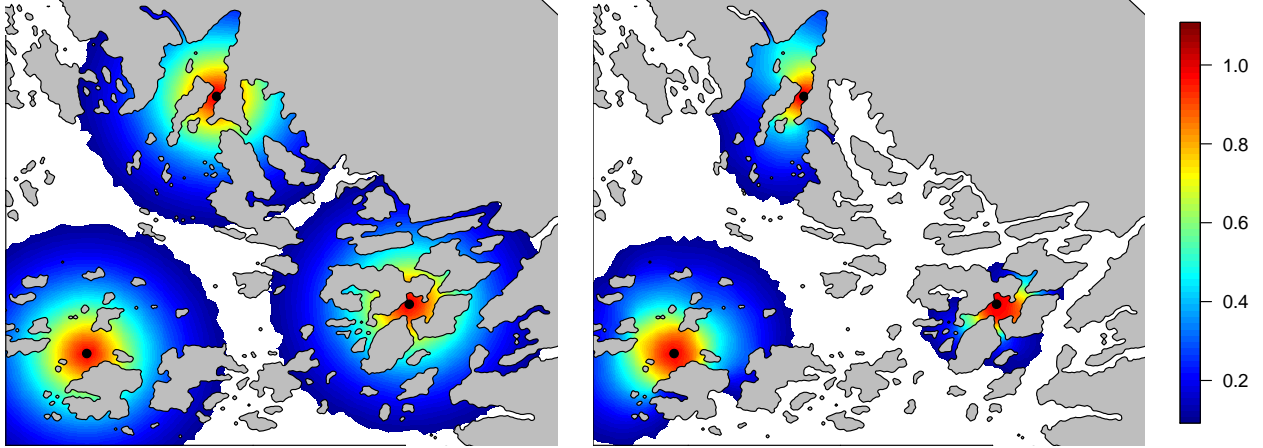


Figure 2: This figure shows the prior behaviour of the new non-stationary Matérn field versus that of the stationary alternative. The map used is for the case study, where water (white area) is considered as normal terrain, and land (grey area) is considered a barrier. The left plot shows three correlation surfaces for the stationary model with range $r = 10\text{km}$. A correlation surface is the prior correlation between any point in the plane and a chosen central point (black dot). The correlation was cut off at 0.1. The right plot shows three correlation surfaces for the non-stationary model, using the same range $r = 10\text{km}$ in the water area, and barrier range $r_b = 2.5\text{km}$. See appendix B for a discussion on r_b . We note how the correlation is forced around barriers, and hindered by the presence of many small islands.

model does exactly what it is supposed to. The barrier model hinders correlation between points with a lot of land mass in between, and almost completely removes correlation between points that cannot be joined by a path through water. Moreover, the effective distance between two locations, measured in terms of how the correlation decreases when moving between them, travels around the barriers. The coefficient r_b must be chosen small enough that the barrier intuitively acts like a barrier, but not so small that we get numerical instabilities when solving the equations. In the application we consider here, $r_b = 2.5\text{km}$ is a good choice. For details about this difficulty, and how we set this parameter, see Appendix B.

For the standard deviation of the field at a location $u(s_i)$ we have two options. One is to use the spatially varying standard deviation we get from solving the above equations, with our fixed barrier range, see Figure 3. This has a higher prior standard deviation in the inlets. The second option is to rescale the precision matrix so that all the marginal standard deviations are 1. This is slightly more computationally demanding, as one would need to find the inverse diagonal of a sparse matrix. In this paper we have chosen the first option, mainly for its interpretation, with the smaller computational cost being a nice bonus. For interpretation, we believe that this non-constant marginal spatial uncertainty is *a priori* reasonable. The spatial random effect is a solution to a stochastic partial differential equation and, hence, represents the “average location” of a randomly moving individual in the physical space defined by the differential equation. Narrow inlets are places that the individual has lower probability to visit compared to large open sea areas but if the individual got into an inlet, it would be stuck there for several steps. This leads to higher standard deviations compared to a stationary model; i.e. either there is a lot of fish, or there are almost no fish, in the inlet.

Before we conclude this subsection there is one important property of the model that we want to highlight. See Figure 4 for an illustration of how correlation seeps out through the gap in a barrier. This shows that the barrier models introduced here are very different from models based on the shortest path. The physical intuition for SDMs is that the smaller a gap is the less likely it is that the individuals find and traverse it. An intelligent agent with an exact map about the area would be

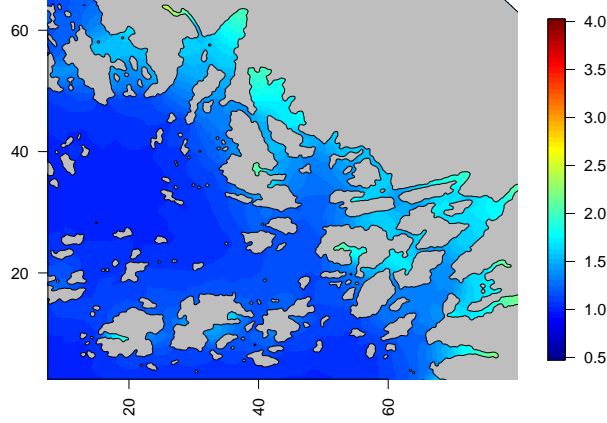


Figure 3: Example prior marginal standard deviation of the spatial effect, using range 20km in the water and range 2.5km on land.

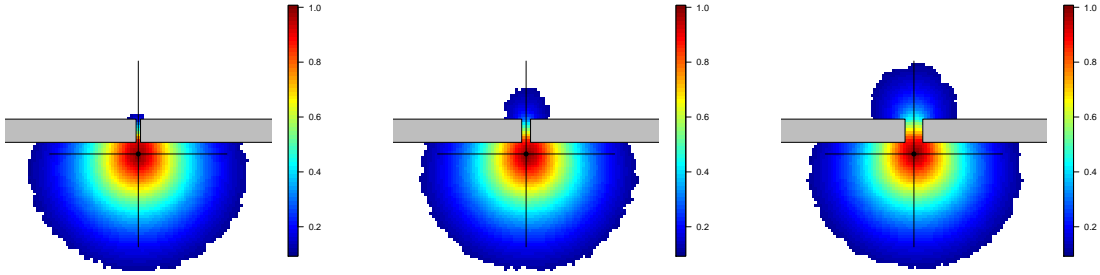


Figure 4: Correlation plots of the barrier model where there is a gap in the barrier. All parameters in the three plots are the same, except the gap widths, which takes the values (0.1, 0.2, 0.4). The black lines illustrate the spatial range (i.e. how far away from the central location that a stationary field would reach before the correlation has decreased to 0.1). This figure shows how the barrier model is different from a shortest-path model (which would not give different behaviour for different gap widths).

able to pick the global shortest path when going from one place to another, but the spatial random effect with barrier can be seen to describe agents that do not have a map and hence randomly search for places to go. These kind of random movements will make an individual much less likely to find themselves on the other side of a small gap.

3.4 Priors for hyper-parameters

We use the following priors for the hyper-parameters

$$\pi(\sigma_\epsilon) \sim \lambda_\epsilon e^{-\lambda_\epsilon \sigma_\epsilon} \quad (8)$$

$$\pi(\sigma_u) \sim \lambda_0 e^{-\lambda_0 \sigma_u} \quad (9)$$

$$\pi\left(\frac{1}{r}\right) \sim \lambda_1 e^{-\lambda_1 \frac{1}{r}}, \quad (10)$$

where the choice of λ s depends on the problem's scale and the user's desire for shrinkage. In this section we discuss the reasoning behind choosing these priors, and define λ s for our case study.

We consider it appropriate to set priors based on *prior modeling preferences*. With this we do not mean that you can elicit the prior completely from *a priori* information about the parameter, but by *a priori* information about how you want the model to behave. As is common in applied models, SDMs are not looking at one specific parameter of interest, but rather several different parameters and a diverse range of possible prediction scenarios. Our focus then is to avoid overfitting, and to ensure that simple models are recovered when they are true (i.e. we are more concerned about estimating the parameters correctly when the true value represents a simpler model). First, we will discuss the chosen priors as shrinkage priors, then we will consider if this is consistent with the interpretation of the hyper-parameters, and we will set the λ parameters.

To construct shrinkage priors, we need

1. the concept of a base model, that is, a simple model to shrink towards,
2. an understanding of what models are essentially the same, and what models are different, so that one can have a meaningful way of choosing the shape of the shrinkage prior
3. a degree of shrinkage that may vary between applications (e.g. essential for taking into account the scale at which data is measured, and the number of competing model components).

A good way to achieve these goals is found in Simpson et al. (2014), which is built upon by Fuglstad et al. (2015) to give priors for range and standard deviation of a Matérn field. Using their results, we get the priors in equation (10), with the following details.

1. The base model is $\sigma_\epsilon = 0, \sigma_u = 0$, and $r = \infty$
2. Distance from the base model, as measured by the square root of the Kullback-Leibler divergence, is a parameter where an exponential prior is reasonable
3. The strength of shrinkage is chosen by setting λ 's

Now for the question of whether these priors are in line with the interpretation of our model. When including an additive component in the linear predictor, one must have an understanding of what structure it is supposed to model. This understanding naturally leads us to prefer some model components for modeling the structure of the data. In general, we strongly prefer modeling variation (in log intensity) with the fixed effects over using random effects, which leads to shrinkage priors for the variance parameters $\sigma_u, \sigma_\epsilon$. The strength of this preference is tuned by λ (e.g. small values of λ lead to significant use of random effects, which possibly leads to weaker conclusions about the fixed effects).

For the size of a model component, we believe that σ is a very good and interpretable parametrization since it has the same units as the linear predictor, and since $\sigma \approx 0$ represents the removal of the model component. The exponential distribution is reasonable prior due to its memorylessness property, which represents the idea that additional randomness should be penalized in the same way, independent of how much randomness you have already included in the model.

The two random effects, the iid effect ϵ and the spatial effect u , are both representing noise in observations, noise in covariate measurements, species aggregation, and missing covariates, respectively, in a local or spatially correlated manner. *A priori* we do not know whether the local or spatially correlated effect should dominate; this leads us to having no preference between the two model components, and so $\lambda_\epsilon = \lambda_0$. To determine the value of λ_ϵ we look at the maximum size of the iid random effect. We believe that the iid effect should be able to explain any datapoint on its own, but that it should be *a priori* extremely difficult, say with a probability of 0.01. The maximum logarithmic value of our measurement counts is from around 4 to around 5 in the three datasets. Because we have an intercept in the model, we think the random effect should only need to extend

up, or down, 3 logarithmic units (we use the natural logarithm) in any of the datasets. We compute the marginal distribution

$$\pi(\epsilon_i) = \int \pi(\epsilon_i|\sigma)\pi(\sigma) d\sigma$$

numerically and define $\lambda_\epsilon = 1.5$ to get the 1% and 99% quantiles approximately at -3 and 3.

This choice is obviously somewhat arbitrary, and different ways of reasoning will give different values. We found values from 0.9 all the way to 2 to be reasonable. However, the results are not unduly influenced by this, since the models with $\lambda = 0.9$ or $\lambda = 2$ give reasonably close parameter estimates to that of the chosen model ($\lambda_\epsilon = 1.5$). Further, this paper’s main focus is on comparing the stationary and the barrier model, where we use the same priors in both models.

For the range r of the spatial effect we have a prior preference for longer range. That is because, by definition, the spatial effect is there to pick up non-local variability. In truth, we expect there to be variability at several different spatial scales, but the spatial effect is supposed to pick up the long range dependencies, leaving the very short range dependencies to the iid effect. However, we want the prior to be weak, so that it is dominated by the likelihood when the short scale spatial structure is the most important for explaining the observations. From a practical point of view, the parametrization $1/r$ can seem strange, and the r parameter can seem more natural. The problem with the r parameter is that the model $r = 1$ and the model $r = 2$ seem very close, but they are very different models, with very different behavior. And although $r = 10$ and $r = 20$ seem very far apart ($\Delta r = 10$), the difference between the behavior at these values are less than the difference between the behavior at $r = 1$ and $r = 2$. The $1/r$ parametrization solves these issues neatly. In this parametrization it is also possible to see when the posterior is leaning towards the base model ($\frac{1}{r} \approx 0$).

For setting λ_1 we first need to ballpark the typical length of the study area. Then we claim that half of this typical length is a decent choice for the prior median of the range, because when sampling spatial fields with this range, the fields seem to be reasonable models of long range spatially structured ecological effects. In the case study, the typical length is 60km, giving prior median range 30km, and $\lambda_1 = 20.8\text{km}$. Additionally, we have a consideration about the tail behavior of the prior. There is a point at which the chosen mesh discretization is not adequate; around $r = 4\text{km}$ we consider the spatial model to have failed to produce reasonable results (this can be fixed by using a finer mesh).

We leave the topic of priors with a few additional notes. We have chosen to use the same prior in the stationary model and in the barrier model. Looking at figure 2 it would also be reasonable to use a slightly larger λ_1 in the barrier model, estimating a slightly longer range. Informally, we recommend these priors, or the equivalent likelihood penalties, as in our experience they make the posteriors better behaved, and stabilize the inference in applications with Poisson observation models.

4 The distribution of smelt larvae in the Archipelago Sea in the South-West coast of Finland

We now discuss the analysis of the smelt larvae data presented in Section 2. The results for the other species were similar. We will compare three models: \mathcal{M}_I denotes the model without spatial field (i.e. $\sigma_u = 0$), \mathcal{M}_S denotes the model with a stationary spatial field, and \mathcal{M}_B denotes the barrier model (non-stationary spatial field) (see Section 3.3). We conduct the inference using **R-INLA** (see www.r-inla.org Rue et al., 2009; Martins et al., 2013).

Figure 5 summarizes the point estimates and 95% credible intervals for the fixed effects. There is a notable differences between the estimates in the stationary model and in the barrier model. These differences are significant compared to the difference between the \mathcal{M}_I model and the spatial models, and therefore the importance of having a non-stationary barrier model is of a similar order as the importance of having a spatial model at all, when estimating fixed effects.

AverageDepth has a large and somewhat significant negative influence on the abundance of smelt larvae, for all three models. This shows that smelt larvae prefer to live close to land and shallow water areas. RiverFlow has a large and significant positive influence in all models, and its effect changes quite a lot from \mathcal{M}_I to spatial models, but not much between the spatial models. We would suggest investigating river flow in future studies, as it may have a real positive effect on the smelt larvae abundance. Openness has a medium size negative effect, which is statistically at most weakly significant. The mean estimate of the effect is greater (in absolute terms) in the models with spatial random effect than in the \mathcal{M}_I model.

From the model comparison point of view the most interesting covariates are Dist30m, TempSum and ShoreDens. Dist30m is almost significant in the \mathcal{M}_I model, but not significant in the two spatial models, and with \mathcal{M}_S its estimated effect is closer to zero. This means that Dist30m is heavily confounded with the spatial effects and that its explanatory power is not much better than the explanatory power of spatial noise. This is reasonable since the pattern in Dist30m resembles well the prior assumptions on the spatial fields (especially in the stationary field), since Dist30m changes very smoothly, in general increasing from south-west to north-east. Similarly, the effect of TempSum is smaller in models with spatial random effect than in the \mathcal{M}_I model. This is reasonable for the same reason as for Dist30m since TempSum describes the sum of daily sea surface temperatures which, on a broad scale, increase from outer sea areas (south-west) towards the main land (north-east). However, the effect of TempSum is smaller in \mathcal{M}_B than in \mathcal{M}_S , showing the opposite behavior to that of Dist30m, where the effect was higher for \mathcal{M}_B . The likely reason for this is that TempSum has a stronger local pattern around the islands and peninsulas than Dist30m. The TempSum may change considerably in very short (Euclidean) distance when moving, e.g., from large open sea area across a peninsula to a sheltered inlet, which is behavior similar to the spatial random effect with barriers. ShoreDens has a large and significant negative effect in the \mathcal{M}_I model and in the \mathcal{M}_B model but its effect is not significant in the \mathcal{M}_S model. The difference in the estimated for \mathcal{M}_B and \mathcal{M}_S is likely a result of how ShoreDens has been constructed. It summarizes the shoreline length inside a 15 km circle and hence varies along the Euclidean coordinates in a similar way as the stationary spatial random field. These three variables illustrate that the influence of the change from stationary to barrier model may affect which covariates are inferred to be statistically significant.

We will now look at the distribution of variance components in the models. See Table 2 for the posterior quantiles of the hyper-parameters. Clearly, σ_ϵ is reduced when a spatial effect is included in the model. This is because some of the noise is explained as spatial noise or as fixed effect structure. Similarly, both with and without covariates, the σ_ϵ noise component is slightly reduced when the barrier effect is used, compared to the stationary spatial effect. In addition, there is a large reduction in the magnitude σ_u of the spatial effect when the barrier model is used instead of the stationary model. This might reflect that the barrier effect is able to explain the same amount of structure in the data with less effort, i.e. that it fits the data in a more parsimonious way, requiring less in the way of size of the model components.

The posterior spatial effects are shown in figure 6 and figure 7. We have included the results from the model without and with covariates, so the reader can consider both the benefits in a pure spatial interpolation application, and the benefits for the full covariate model. Here we see that the stationary model smooths over land compared to the barrier model. In the south-east part of these plots we find inlets, where we observe significantly more uncertainty in the barrier model compared to the stationary model. This is in accordance with our intuition, as we do not have much information about what happens there, because the barrier (i.e. land) is separating the inlets from nearby measurement locations.

We have computed two model comparison criteria, DIC (Deviance Information Criterion) and WAIC (Widely Applicable Information Criterion), see Spiegelhalter et al. (2014) for a discussion of these two criteria. The results are in Table 3. The literature on model comparison is extensive, and different criteria have different strengths and weaknesses. A big issue in the applied context is that we are not after one specific goal, e.g. we are not after having optimal predictions for new observations

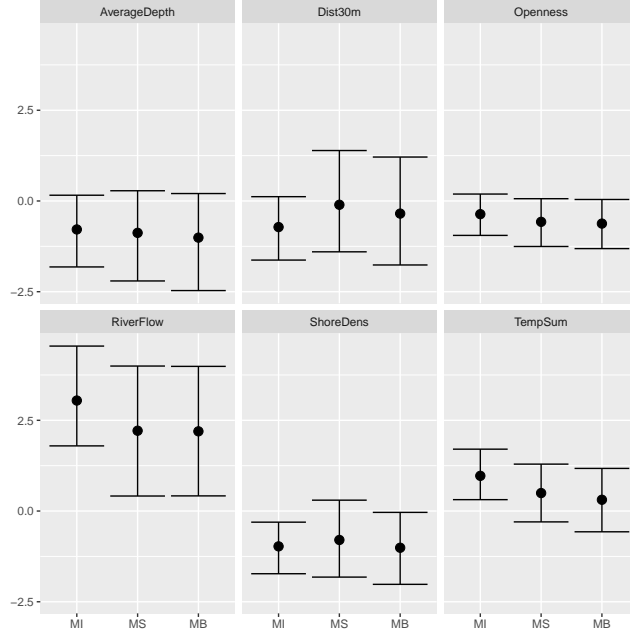


Figure 5: A comparison of the posterior medians and 95% credible intervals of the fixed effects in the smelt analysis between the three models. \mathcal{M}_I denotes the model without spatial field, \mathcal{M}_S denotes the model with stationary spatial field, and \mathcal{M}_B denotes the model with (non-stationary) spatial field with barriers (see Section 3).

Covariates	Model	Range r	σ_u	σ_ϵ
No	\mathcal{M}_I	-	-	3.09 (2.51, 3.87)
No	\mathcal{M}_S	55.3 (26.6, 118)	3.45 (2.22, 5.45)	1.34 (0.97, 1.85)
No	\mathcal{M}_B	44.3 (22.9, 106)	1.85 (1.3, 2.84)	1.29 (0.95, 1.78)
Yes	\mathcal{M}_I	-	-	1.85 (1.42, 2.43)
Yes	\mathcal{M}_S	15.5 (5.7, 45)	1.39 (0.76, 2.49)	1.37 (0.93, 2.04)
Yes	\mathcal{M}_B	16.6 (5.8, 51)	0.95 (0.49, 1.81)	1.33 (0.88, 2.04)

Table 2: Posterior quantiles of hyperparameters for the smelt data, using median and (0.025, 0.975) quantiles. For interpreting the range parameter, we keep in mind that the measurement locations are spread over a 58km by 70km area.

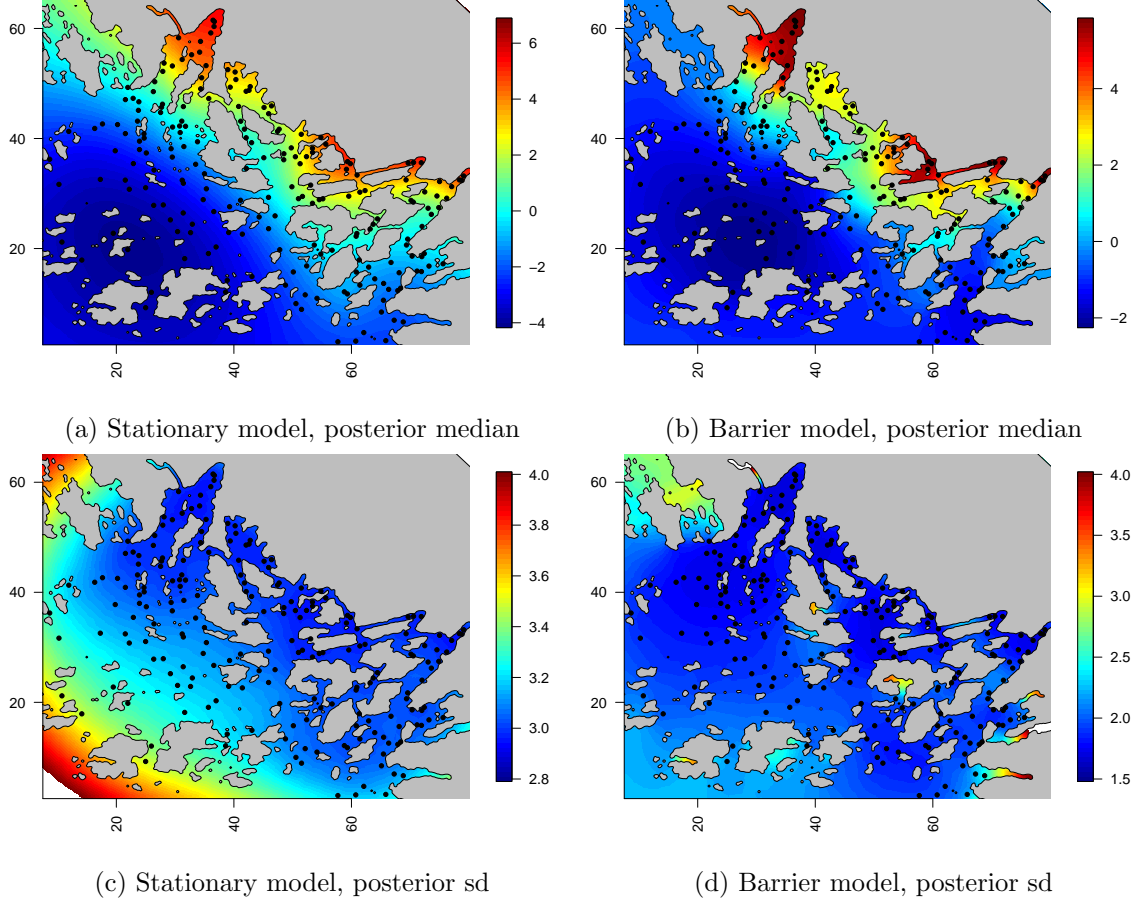


Figure 6: Posterior of the spatial field for the smelt larvae in the spatial models without covariates. We see how the stationary model oversmooths in the northern part of the figure compared to the barrier model. We see that the uncertainty in the barrier model is larger in inlets where there are no nearby observations.

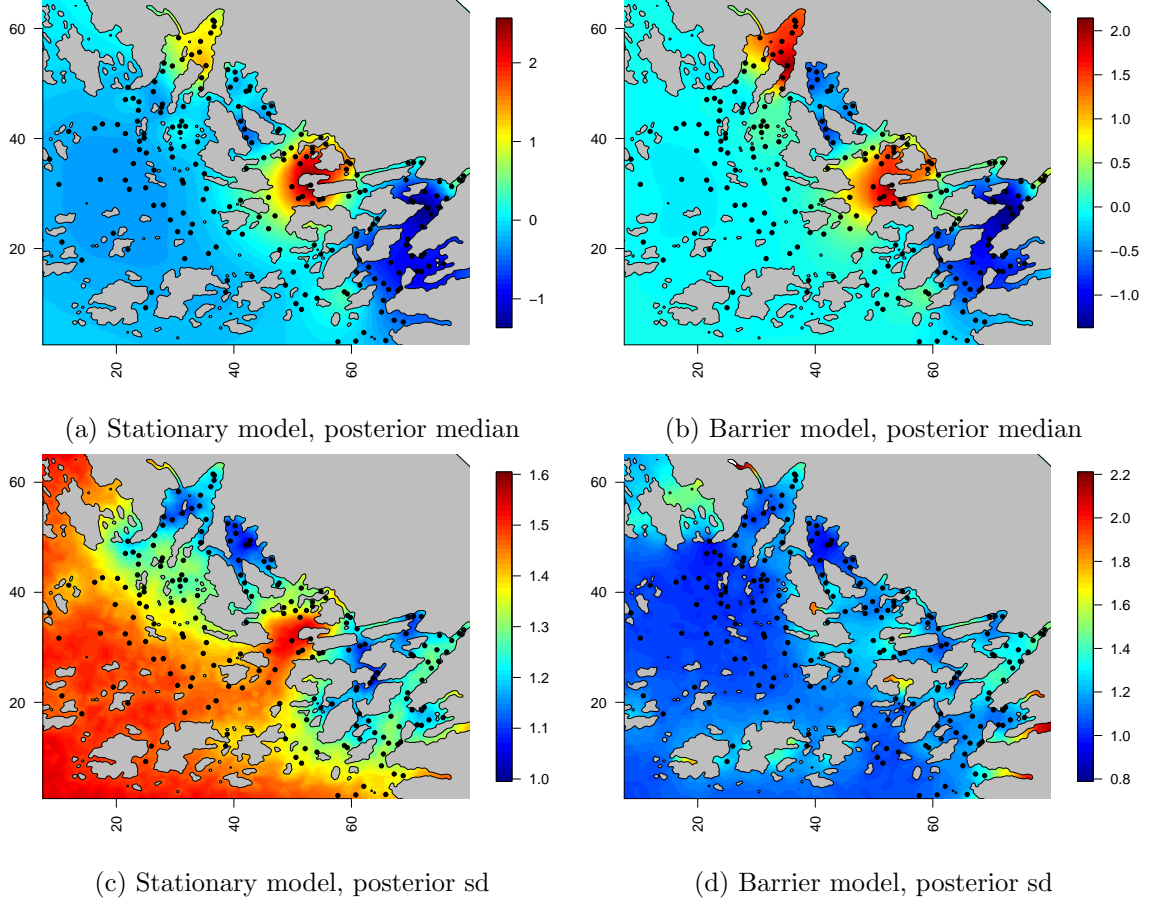


Figure 7: Posterior of the spatial field for the smelt larvae in the spatial models with covariates. We see how the stationary model oversmooths in the northern part of the figure compared to the barrier model. We see that the uncertainty in the barrier model is larger in inlets where there are no nearby observations.

Species	Covar	Model	DIC	WAIC
Smelt	No	\mathcal{M}_I	369	441
Smelt	No	\mathcal{M}_S	319	318
Smelt	No	\mathcal{M}_B	318	313
Smelt	Yes	\mathcal{M}_I	316	316
Smelt	Yes	\mathcal{M}_S	316	314
Smelt	Yes	\mathcal{M}_B	316	313
Pikeperch	No	\mathcal{M}_I	534	560
Pikeperch	No	\mathcal{M}_S	428	423
Pikeperch	No	\mathcal{M}_B	429	416
Pikeperch	Yes	\mathcal{M}_I	438	428
Pikeperch	Yes	\mathcal{M}_S	426	413
Pikeperch	Yes	\mathcal{M}_B	430	417
Perch	No	\mathcal{M}_I	248	242
Perch	No	\mathcal{M}_S	213	206
Perch	No	\mathcal{M}_B	214	208
Perch	Yes	\mathcal{M}_I	212	209
Perch	Yes	\mathcal{M}_S	211	208
Perch	Yes	\mathcal{M}_B	211	209

Table 3: Model comparison on each of the 3 different data-sets, with 6 models on each. DIC is Deviance Information Criterion, and WAIC is Widely Applicable Information Criterion.

that are very similar to that of our dataset. We are, however, interested in having *good* predictions in that situation. In other words, there is no one single prediction scenario we wish to perform optimally, but rather, a host of possible prediction scenarios that we want to do well at. In this paper we have chosen two measures that are easy to compute within the **INLA** framework, requiring a negligible computational effort. We will consider any model bad if it is significantly worse, in both model comparison measures, than the model(s) with the best score. Here, the word significant is not well defined, but we use our expert opinions of what is a clearly significant difference in these measures. From this we conclude that the iid model without any covariates is a bad model, for any of the three species. The DIC and WAIC is not able to clearly differentiate between the appropriateness of any of the other models for any of the three species.

5 Discussion

When fitting a limited amount of data, the prior modeling assumptions heavily impact the conclusions. In these cases it is very important to choose a realistic model for the spatial random effect. For the case study presented here, basic intuition tells us that the common assumption of stationarity in the spatial effect might be inappropriate. To remedy this, we developed a spatial model that takes into account the existence of spatial barriers in the study area. We investigated the model's prior behavior and found it appropriate. An application of the non-stationary model to the spatial distribution of fish larvae in an archipelagic region on the Finnish coast showed a clear impact on inference and results. Going from a stationary model to the barrier model significantly changes the inference results; the fixed effect estimates and credible intervals change, and the posterior standard deviations of the spatial field and iid effect change. This, in turn, will have a substantial influence on predictions, both within the study area and in an extrapolation to other areas.

The methodology we have developed will be very useful to species distribution modeling in general, as there are physical, geographical and topographical barriers commonly present in many study

systems, especially in larger scale studies. In addition to land being a barrier for aquatic animals, roads and power-lines may be a barrier to reindeer and wild animals, industrial areas may be a barrier when measuring health or population indices, human settlements may be a barrier to bird movements, and sea is a barrier to land based animals.

This method was developed with a focus on usability by practitioners, e.g. biologists and ecologists. It is based on one of the common inference tools in spatial statistics, namely the R package **R-INLA**. It is simple for a practitioner to use this functionality, given that they are already familiar with **R-INLA**. The only extra step needed, compared to fitting a stationary model, is to specify which part of the study area is the barrier area, e.g. by a polygon or raster. At www.r-inla.org/barrier-model we provide tutorial and code examples, which will be extensively updated in the near future.

6 Bibliography

References

- Austin, M. (2007). Species distribution models and ecological theory: A critical assessment and some possible new approaches. *Ecological Modelling*, 200(1-2):1–19.
- Bergström, U., Sundblad, G., Sandström, A., and Eklöv, P. (2014). Nursery habitat availability limits adult stock sizes of predatory coastal fish. *ICES Journal of Marine Science*, 71:672–680.
- Clark, J. S., Gelfand, A. E., Woodall, C. W., and Zhu, K. (2014). More than the sum of the parts: Forest climate response from joint species distribution models. *Ecological Applications*, 24(5):990–999.
- Dijkstra, E. W. (1959). A note on two problems in connexion with graphs. *Numerische mathematik*, 1(1):269–271.
- Elith, J. and Leathwick, J. R. (2009). Species distribution models: Ecological explanation and prediction across space and time. *Annual Review of Ecology, Evolution, and Systematics*, 40:677–697.
- Fuglstad, G.-A., Simpson, D., Lindgren, F., and Rue, H. (2015). Interpretable priors for hyperparameters for gaussian random fields. *arXiv preprint arXiv:1503.00256*.
- Gelfand, A. E., Diggle, P. J., Fuentes, M., and Guttorp, P. (2010). *Handbook of Spatial Statistics*. CRC Press.
- Gelfand, A. E., Silander Jr., J. A., Wu, S., Latimer, A., Lewis, P. O., Rebelo, A. G., and Holder, M. (2006). Explaining species distribution patterns through hierarchical modeling. *Bayesian Analysis*, 1:41–92.
- Guisan, A., Edwards, T. C., and Hastie, T. (2002). Generalized linear and generalized additive models in studies of species distributions: setting the scene. *Ecological Modelling*, 157(2-3):89–100.
- Higdon, D. (1998). A process-convolution approach to modelling temperatures in the north atlantic ocean. *Environmental and Ecological Statistics*, 5:173–190.
- Johnston, A., Fink, D., Reynolds, M. D., Hochachka, W. M., Sullivan, B. L., Bruns, N. E., Hallstein, E., Merrifield, M. S., Matsumoto, S., and Kelling, S. (2015). Abundance models improve spatial and temporal prioritization of conservation resources. *Ecological Applications*, 25(7):1749–1756.
- Kallasvuori, M., Vanhatalo, J., and Veneranta, L. (2016). Modeling the spatial distribution of larval fish abundance provides essential information for management. *Canadian Journal of Fisheries and Aquatic Sciences*, conditionally accepted.

- Kennedy, M. C. and O’Hagan, A. (2001). Bayesian calibration of computer models. *Journal of the Royal Statistical Society: Series B (Statistical Methodology)*, 63(3):425–464.
- Latimer, A. M., Wu, S., Gelfand, A. E., and Silander, Jr., J. A. (2006). Building statistical models to analyze species distributions. *Ecological Applications*, 16(1):33–50.
- Lindén, A. and Mäntyniemi, S. (2011). Using the negative binomial distribution to model overdispersion in ecological count data. *Ecology*, 92:1414–1421.
- Lindgren, F., Rue, H., and Lindström, J. (2011). An explicit link between gaussian fields and gaussian markov random fields: the stochastic partial differential equation approach. *Journal of the Royal Statistical Society: Series B (Statistical Methodology)*, 73(4):423–498.
- Martins, T. G., Simpson, D., Lindgren, F., and Rue, H. (2013). Bayesian computing with inla: new features. *Computational Statistics & Data Analysis*, 67:68–83.
- Ovaskainen, O., Abrego, N., Halme, P., and Dunson, D. (2015). Using latent variable models to identify large networks of species-to-species associations at different spatial scales. *Methods in Ecology and Evolution*.
- Paciorek, C. and Schervish, M. (2006). Spatial modelling using a new class of nonstationary covariance functions. *Environmetrics*, 17:483–506.
- Ramsay, T. (2002). Spline smoothing over difficult regions. *Journal of the Royal Statistical Society: Series B (Statistical Methodology)*, 64(2):307–319.
- Rue, H., Martino, S., and Chopin, N. (2009). Approximate bayesian inference for latent gaussian models by using integrated nested laplace approximations. *Journal of the Royal Statistical Society: Series B (Statistical Methodology)*, 71(2):319–392.
- Scott-Hayward, L. A. S., MacKenzie, M. L., Donovan, C. R., Walker, C., and Ashe, E. (2014). Complex region spatial smoother (cress). *Journal of Computational and Graphical Statistics*, 23(2):340–360.
- Shpilev, H., Ojaveer, E., and Lankov, A. (2005). Smelt (*Osmerus eperlanus* L.) in the baltic sea. *Proceedings of the Estonian Academy of Sciences, Biology and Ecology*, 54:230–241.
- Simpson, D. P., Martins, T. G., Riebler, A., Fuglstad, G.-A., Rue, H., and Sørbye, S. H. (2014). Penalising model component complexity: A principled, practical approach to constructing priors. *arXiv preprint arXiv:1403.4630*.
- Spiegelhalter, D. J., Best, N. G., Carlin, B. P., and Linde, A. (2014). The deviance information criterion: 12 years on. *Journal of the Royal Statistical Society: Series B (Statistical Methodology)*, 76(3):485–493.
- Vanhatalo, J., Veneranta, L., and Hudd, R. (2012). Species distribution modelling with gaussian processes: a case study with the youngest stages of sea spawning whitefish (*Coregonus lavaretus* L. s.l.) larvae. *Ecological Modelling*, 228(0):49 – 58.
- Wood, S. N., Bravington, M. V., and Hedley, S. L. (2008). Soap film smoothing. *Journal of the Royal Statistical Society: Series B (Statistical Methodology)*, 70(5):931–955.

A Solving the SPDE and computing the precision matrix Q

In this appendix we detail how to solve our particular stochastic partial differential equation with a finite element method based on linear elements. Solving the equation results in a precision matrix Q for the Gaussian spatial random effect, i.e.

$$\vec{u} = \mathcal{N}(0, \sigma_u^2 Q^{-1}).$$

We follow the process in the SPDE paper by Lindgren et al. (2011) for making a GMRF approximation to the Gaussian field. To facilitate fast computations we aim for a very sparse structure in Q . In this appendix you find clarifications and some additional details for our special case, hopefully making it a useful addition to the paper by Lindgren et al. (2011). However, we do assume some familiarity with partial differential equations and the Finite Element method.

The system to be solved by a Finite Element method is

$$\begin{aligned} \left[1 - \nabla \frac{r(s)^2}{8} \nabla\right] u(s) &= r(s) \sqrt{\frac{\pi}{2}} \mathcal{W}(s) \\ r(s) &= r_q \text{ on } \Omega_q, \text{ alternatively written as} \\ r(s) &= \sum_{q=1}^k r_q 1_{\Omega_q}(s) \end{aligned}$$

where the domain Ω is a disjoint union of Ω_q for $q = 1, 2, \dots, k$, and with Neumann boundary condition on $\partial\Omega$. This is a minor generalisation; we have used $k = 2$ in this paper.

The goal is to find a matrix equation

$$A\vec{u} = \vec{\epsilon}$$

where A and $\vec{\epsilon}$ are known.

The Finite Element method (linear elements) requires us to first specify a mesh, i.e. a triangulation, of the domain. Here we require that any triangle is contained in only one Ω_q . This is a modeling assumption that gives a unique way to solve the equation using linear finite elements. As the mesh resolution gets finer, the boundaries between the different Ω_q should be resolved more precisely. Without further comment, we assume the standard properties of the mesh and boundary; that they are both "nice" in the way required for convergence of the numerical solution. The linear elements are denoted $\psi_i(s)$ and take the value 1 at node i , and zero at all other nodes, with a linear decay from node i to its neighbours. They are also known as hat-function, since they look like linear hats.

The vector \vec{u} of values u_i (for the GMRF) can be thought of in two ways

$$\begin{aligned} u(s_i) &= u_i, \\ u(s) &= \sum_{i=1}^N u_i \psi_i(s), \end{aligned}$$

both as the values at the nodes s_i in the mesh, and as "how many replicates of each hat-function do you consist of?" Here, N is the total number of mesh nodes. The observation locations can be anywhere in the mesh.

When solving this SPDE with finite elements, the equation is re-interpreted in the following weak form,

$$\left\langle \psi_j(\cdot), \left[1 - \nabla \frac{r(\cdot)^2}{8} \nabla\right] u(\cdot) \right\rangle = \left\langle \psi_j(\cdot), r(\cdot) \sqrt{\frac{\pi}{2}} \mathcal{W}(\cdot) \right\rangle,$$

for all j , where the inner product is

$$\langle f, g \rangle = \int f(s)g(s) \, ds.$$

Writing $u(s)$ as a linear combination of elements, and putting the resulting coefficients into matrix form, we get the following.

$$\begin{aligned} A\vec{u} &= \vec{\epsilon} \\ A &= [J - \frac{1}{8} \sum_{q=1}^k r_q^2 D_q] \\ J_{i,j} &= \langle \psi_i, \psi_j \rangle = \int \psi_i(s)\psi_j(s) \, ds \\ (D_q)_{i,j} &= \langle 1_{\Omega_q} \nabla \psi_i, \nabla \psi_j \rangle = \int_{\Omega_q} \nabla \psi_i(s) \nabla \psi_j(s) \, ds \\ C &= \text{Cov}(\vec{\epsilon}) \\ \tilde{C} &= \frac{\pi}{2} \sum_{q=1}^k r_q^2 \tilde{C}_q \\ (\tilde{C}_q)_{i,i} &= \langle 1_{\Omega_q} \psi_i, 1 \rangle = \int_{\Omega_q} \psi_i(s) \, ds \end{aligned}$$

where \tilde{C}_q are diagonal matrices, so ϵ_i are independent. To get the approximation \tilde{C} of C , we follow the arguments in the SPDE paper by Lindgren. Using that A is symmetric, we get

$$\begin{aligned} Q &= \text{Prec}(\vec{u}) \\ Q &= A\tilde{C}^{-1}A \end{aligned}$$

In the final algorithm, we have done no additional approximations. In the way the regions and $r(s)$ are defined, this is a straight-forward FEM implementation. For computational efficiency it is important to store the matrices J, C_q , and D_q so that Q can be computed quickly for new values of $(r_q)_q$.

A standard part of model checking is to refine the grid (add more mesh nodes) to see whether the results are sensitive to the grid. Increasing the number of spatial nodes gives a better approximation to the continuous field, but increases the computational burden. In general, even though we get closer to the continuous field this may not necessarily produce a better model for the data. Refining the mesh also improves the approximation of the boundary shapes of the Ω_q , when these shapes are complex.

B Setting the barrier range r_b

Intuitively we wanted to set the range in the barrier region to near 0. But that is not possible. This is because the finite element approximation only works well in the case when the range is several times greater than the maximum length of any edge in the finite element mesh. For example, in our application, the maximum edge length is 1km, with the typical length along the shoreline being less than half this (to get a good approximation of the shoreline). And so, 2.5km is the lowest value where we can be quite confident that the approximation works well.

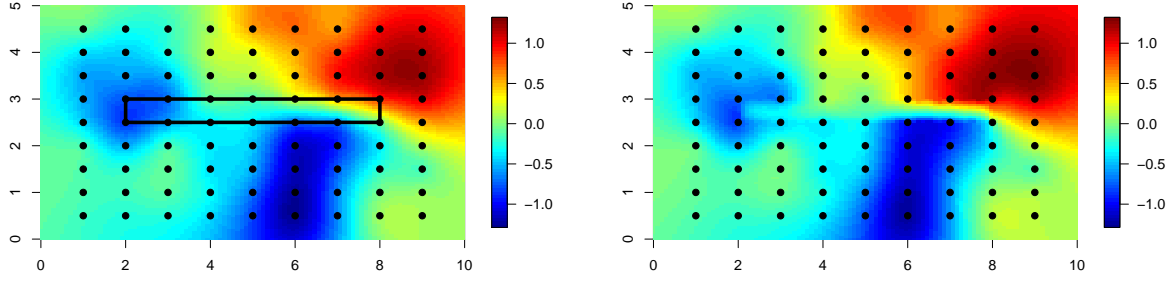


Figure 8: The posteriors for the spatial effects in the single simulation. The stationary field to the left and the Barrier field to the right. The black dots are the measurement locations, the black rectangle is the defined barrier area. Outside of the barrier area we can spot some differences. Inside the barrier area, the field is of no interest, as there will never be data points or prediction locations inside the barrier. The black rectangle was not included in the right plot, as it reduced the visual information.

In general, one might think that fixing this value "to what seems appropriate" is poor statistical methodology. But, as long as one chooses this value by investigating the prior correlation and prior marginal standard deviation plots, this is a perfectly valid method, as we have not introduced the data yet.

When investigating these plots in our case, we see that the prior marginal standard deviation increased where the barrier area was very concave, when we decreased the barrier range. More importantly, we observed that the correlation structure did not change much. From this we conclude that we can use a quite large barrier range in practice, for example 3% of the width of the study area. We did consider whether to rescale the prior spatial fields so that all the marginal standard deviations are 1. This can be done by finding the diagonal of the covariance matrix through a sparse diagonal inverse method, and then just multiplying the precision matrix with a diagonal matrix of these values. That would lead to a slightly different model, which you can argue is either more or less appropriate, while also carrying a heavier computational cost. We found no solid arguments for performing this rescaling.

C Illustration with simulated data

In the smelt larvae analysis, we did not detect a significant change in the predictive measures of fit. We therefore decided to include a small simulation example to show that it is possible to have significant prediction gains by using the new model. The model here consist of only the spatial field with a Gaussian observation likelihood. Figure 8 shows that the posterior mean fields are similar outside of the barrier region. Figure 9 shows the difference between the posterior distributions of the hyper-parameters, where the stationary model undersmooths to compensate for the barrier. Table 4 shows that the difference in predictive scores are significant, hence the difference between the models are of practical significance.

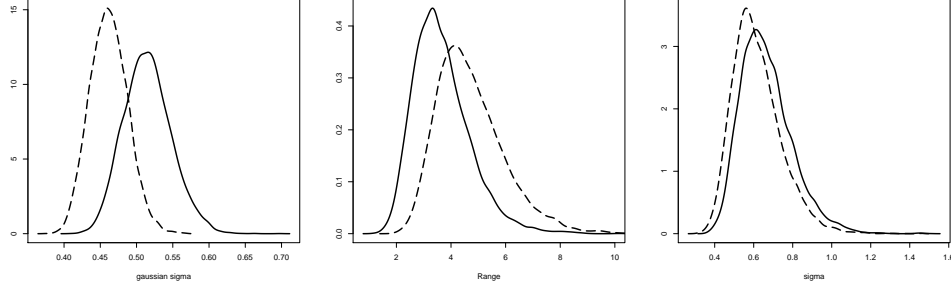


Figure 9: The posteriors for the hyper-parameters in the simulation experiment, Gaussian likelihood noise σ_g , range r and field sd σ_u respectively. Note how the stationary (solid line) range is lower than the barrier (dashed line) range.

Model fit	WAIC	app-log-CV
Stationary	-18	90
Barrier	-88	121

Table 4: The model fit differences when simulating from the barrier model and fitting with a stationary and the barrier model respectively. We note that both the Widely Applicable Information Criterion, and the approximated Leave One Out Cross Validation summed log predictive density (as given by the **INLA** algorithm) is significantly better for the barrier model.